Full Waveform Inversion: Comparison between Different Objective Functionals

Bulcão, A.; Soares Filho, D.M.; Loureiro, F.P.; Alves, G.C.; Farias, F.F.; Santos, L.A.; Petrobras

Abstract

This work compares different types of objective functionals that may be used in the formulation of the inversion methodology called Full Waveform Inversion. The behavior of the inversion scheme is related to the choice of this functional, which provides a measure that quantifies the discrepancy between the observation (real seismic data) and the prediction (simulated data corresponding to a set of model parameters) [FICHTNER, 2010].

For the inversion scheme to converge to an acceptable solution, applying gradient based methods, in a reasonable number of iterations and without being trapped in a local minimum, two factors are important: the space solution topology and its derivatives in relation to the model parameters specified. Both factors are strongly connected to the choice of the employed objective functional [FICHTNER, 2010].

The behaviors of different objective functionals were analyzed using synthetic examples based on the Marmousi model. Data sets were created considering the acoustic wave equation and presence or absence of additive random noise.

Introduction

In seismic imaging the Full Waveform Inversion (FWI) has recently gained much importance, mainly due to advances in computational power and seismic acquisition improvements, especially in areas with high geological complexities. In fact, it can provide higher seismic resolution compared to pre-stack depth migration, which may contribute to better seismic interpretation.

The so called Full Waveform Inversion could understand as an optimization process, where the model parameters are adjusted such that the simulated seismic date better fits the observed one. To simulated the seismic answers, in this work, the two-way acoustic wave equation with constant density were employed, but others more sophisticated equations could be used.

There are several different approaches that could be used to formulate a Full Waveform Inversion scheme, both in terms of time or frequency domain, optimization scheme (steepest descendent, conjugate gradient, quasi-Newton, etc), etc.. . A good review of these different possibilities could be found in Virieux & Operto (2004). In this wok, the frequency domain was used to simulate the seismic data (Hustedt *et al,* 2004) and also the inversion was performed in this domain, using a multi-scale approach, where the result for a lower frequency was used as input for the next frequency.

To obtain the gradient, the direction according the model parameters must be update to obtain a better adjustment with the seismic data, was obtain using the so call Adjoint State Method (Tarantola, 1984; Pratt, 1998), as will be briefly introduce in the next section.

Method

Following the methodology presented by Fichtner (2010), to develop the methodology an objective functional is defined, according to:

$$C(m) = \langle \chi_1(u(m)) \rangle$$

Where: m – is the model parameter, u – is the simulated seismic wavefield at the receiver location, χ_1 - is the kernel of the objective function (expressing a mathematical function that measures the difference between the simulated and observed seismic data); <> - represents a short notation for the integral over time and space.

To avoid the calculation of $\partial u / \partial m$ to obtain the gradient, which is impractical for problems with a large numbers of unknowns (as the Full Waveform Inversion), the Adjoint State Method is employed. Using some mathematical artifices, with an auxiliary wavefield called adjoint wavefield u^+, the gradient could be obtained by:

$$\nabla_m C(m)\delta_m = \langle u^+ . \nabla_m \mathbf{L}\delta_m \rangle$$

Where: $\mathbf{L}$ – represents the direct problem, the partial differential equation used to simulated the seismic response ($\mathbf{L}(u,m) = f$, being f the external forces). The adjoint wavefield is expressed by the following equation:

$$\nabla_u \mathbf{L}^+ u^+ = -\nabla_u \chi_1^+$$

Those are the main steps for the mathematical formulation to obtain the gradient according to a defined objective function. In these work three different objectives functions were investigated (J1, J2 and J3, whose expressions are given below).

The first objective function J1, represents the most traditional functional used in the Full Waveform Inversion, the L2 norm of the residue between the observed (d) and simulated (u) data.

$$J1(m) = \left\langle d \ - \mathrm{M}^{\mathrm{S}} u \ \right\rangle$$

Where: M^s is an operator that select the data at the receivers locations.

The second functional J2, consider an extrapolation (back-propagation) of the residue inside the velocity model.

$$J2(m) = \left\langle \mathbf{L}^{+^{-1}} \mathrm{M}^{\mathrm{D}} \left(f \ - \mathrm{M}^{\mathrm{S}} u \ \right) \right\rangle$$

Where: M^d is an operator that impose the residue at the all the points in the velocity model (reverse of the operator M^s).

The third functional J3, represents the expression of image condition used in the Reverse Time Migration schemes, calculated using the residue.

$$J3(m) = \left\langle u \ \left(\mathbf{L}^{+^{-1}} \mathrm{M}^{\mathrm{D}} \left(f \ - \mathrm{M}^{\mathrm{S}} u \ \right) \right)^{*} \right\rangle$$

For all these three objectives functions the gradients were obtained following the procedures presented before, using the Adjoint State Methods.

Numerical Example

The results of the proposed Full Waveform Inversion schemes will be compared with two different data sets, originated by the Marmousi Velocity Model (depicted in figure 1). Both data sets consider a fixed spread acquisition with receivers along the entire surface and individual sources covering the same positions.

The first data set is a synthetic noise free data, using the acoustic wave equation, discretized using the Finite Difference Method in the Frequency Domain (HUSTEDT *et al*, 2004). For the second one, random noise was added, with a value range of 50% of the maximum amplitude present in the seismogram.

The modeling and inversion parameters employed are presented at table 1. The frequency range for the inversion started at 7.32 Hz up to 24.41 Hz, with 15 different equally spaced values. These frequencies were inverted consecutively in a multi-scale approach, where the previous result for a lower frequency was the input velocity model for the next frequency to be inverted. The initial velocity model for the lowest frequency is shown at figure 2 and was obtained applying twice a moving average 2D filter with 90 grid points over the true velocity model.

All objective functionals presented here were iterated 20 times for each frequency, with the steepest descent algorithm for the optimization scheme. In these cases, the step lengths were calculated so that the maximum velocity update had a fixed module value (50 m/s for the first trial). After the evaluation of the objective functional, if its value did not decrease, the maximum velocity variation for the step length was reduced in 80% until this velocity reaches the limit of 1.0 m/s. This limit is an additional stopping criterion for the inversion in that frequency.

Table 1 – Modeling and Inversion parameters

Grid point interval	12 m
Model dimensions X and Z	384 x 122 grid points
Number of receivers	384
Number of shot gathers	384

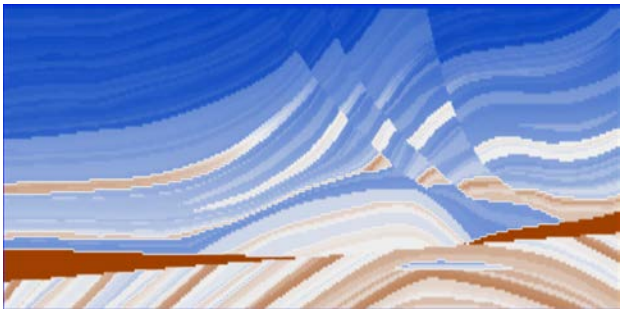

Figure 1 – Marmousi Velocity model.

Figure 2 – Initial Velocity model for the inversions

The results after the end of the inversion schemes for all the 15 frequencies, with only 20 iterations per frequency, are presented in figure 3. The left column shows the final model for the noise free data set and the right one shows results for the model with noise. High resolution in the shallow areas of the model were observed for all objective functionals employed, especially for the noise free data set, with minor differences between them. The biggest variations occurred at the deep and central parts of the model.

Analyzing the images depicted in figure 3 and comparing both data sets, it is advocated that the last objective functional (J3) presents a more stable result, and even that J2 is more stable than J1, despite the fact that the J3 result for the noisy data seems smoother when compared to the other objective functionals. This characteristic of the J3 result may be used as an advantage for lower frequencies in real data applications, where the signal to noise ratio is small at the lowest frequencies and the

corresponding model for these frequencies is already smooth.

It is also claimed that the propagation and back-propagation present in the adjoint source expression for both the J2 and J3 objective functionals helps reduce the effects of noise in the data, because during the extrapolation the wave equation acts as some kind of filter for the incoherent noise.

Figure 4 and table 2 are presented to corroborate those assertions about the objective functionals behavior. Figure 4 shows a highlighted area of the true model (left) and a measure of the square difference between results with and without noise for each objective functional, J1, J2 and J3 (left to right). The values shown are presented in gray scale, with the maximum difference in black. By these results, the lower number of dark regions shows that the functional J3 presents an advantage. The difference between functionals with and without noise are quantified by table 2; where the lower ratio value represents a more stable behavior for the J2 and J3 functionals than for J1 at the presence of random noise.

Table 2 – Objective Functional Values for the last inverted frequency for each case, with and without noise, and also the ratio between them.

	J1	**J2**	**J3**
Noise Free	2431.5e-03	3.3632	0.3306e-06
Noisy	0.0128e-03	29438.0	479.78e-06
Ratio	***52837.06***	***8753.02***	***1451.04***

Table 3 depicts the relative objective functional variation – at the end of 20 iterations – for the lowest frequency and using the same initial model on noise free and noisy data for all cases. It can be seen that the objective functional decreases to roughly the same value (around 1.5% of the initial value) for all functionals on noise free data. However, when noise was added, the J1 functional wasn't capable of significantly reducing the value of the objective functional, unlike J2 and specially the J3 functional. The higher the decrease in the presence of noise, the more stable is the objective functional.

Table 3 – Relative values of the objective functionals for the lowest frequency and using the initial velocity model (figure 2), for both data sets.

	J1	**J2**	**J3**
Noise Free	1.3836 %	1.4996 %	1.5286 %
Noisy	98.4677 %	79.1698 %	63.5816 %

Conclusions

When noise was considered, the results obtained show that selecting different objective functionals the robustness and stability could be improved generating better solution for the inverted parameter (propagation velocity).

The presented results reinforce that Full Waveform Inversion is an outstanding methodology to recover parameters, in this case propagation velocity, through an optimization scheme. The results, starting from a very smoothed initial velocity (figure 2), show the main features (layers and faults) present in the true model and could be used straight into interpretation or to improve the seismic imaging by sequentially apply migration algorithms.

By increasing order, the objective functional that presents a more stable behavior were J2 and J3. In the gradients formulas, for both cases, the adjoint sources expressions have the residual data extrapolation. This extrapolation seems to work as some kind of filter for the random noise, improving the final results when comparing with traditional objective functional J1.

Acknowledgments

The authors would like to thank Petrobras for the permission to publish these results.

References

HUSTEDT, B.; OPERTO, S.; VIRIEUX, J.; 2004, *Mixed-grid and staggered-grid finite-difference methods for frequency-domain acoustic wave modeling*, **Geophysical Journal International**, vol. 157, pages 1269–1296.

FICHTNER, A.; 2010, ***Full seismic waveform modelling and inversion***, Spinger-Verlag, Heidelberg.

VIRIEUX, J., OPERTO, S.; 2009, An overview of full-waveform inversion in exploration geophysics, ***Geophysics***, Vol. 74, No. 6, pp. WCC1-WCC26

TARANTOLA, A., 1984, Inversion of seismic reflection data in the acoustic approximation, ***Geophysics***, 49, 1259–1266.

PRATT, R. G., C. SHIN, AND G. J. HICKS, 1998, Gauss-Newton and full Newton methods in frequency-space seismic waveform inversion: ***Geophysical Journal International***, 133, 341–362.

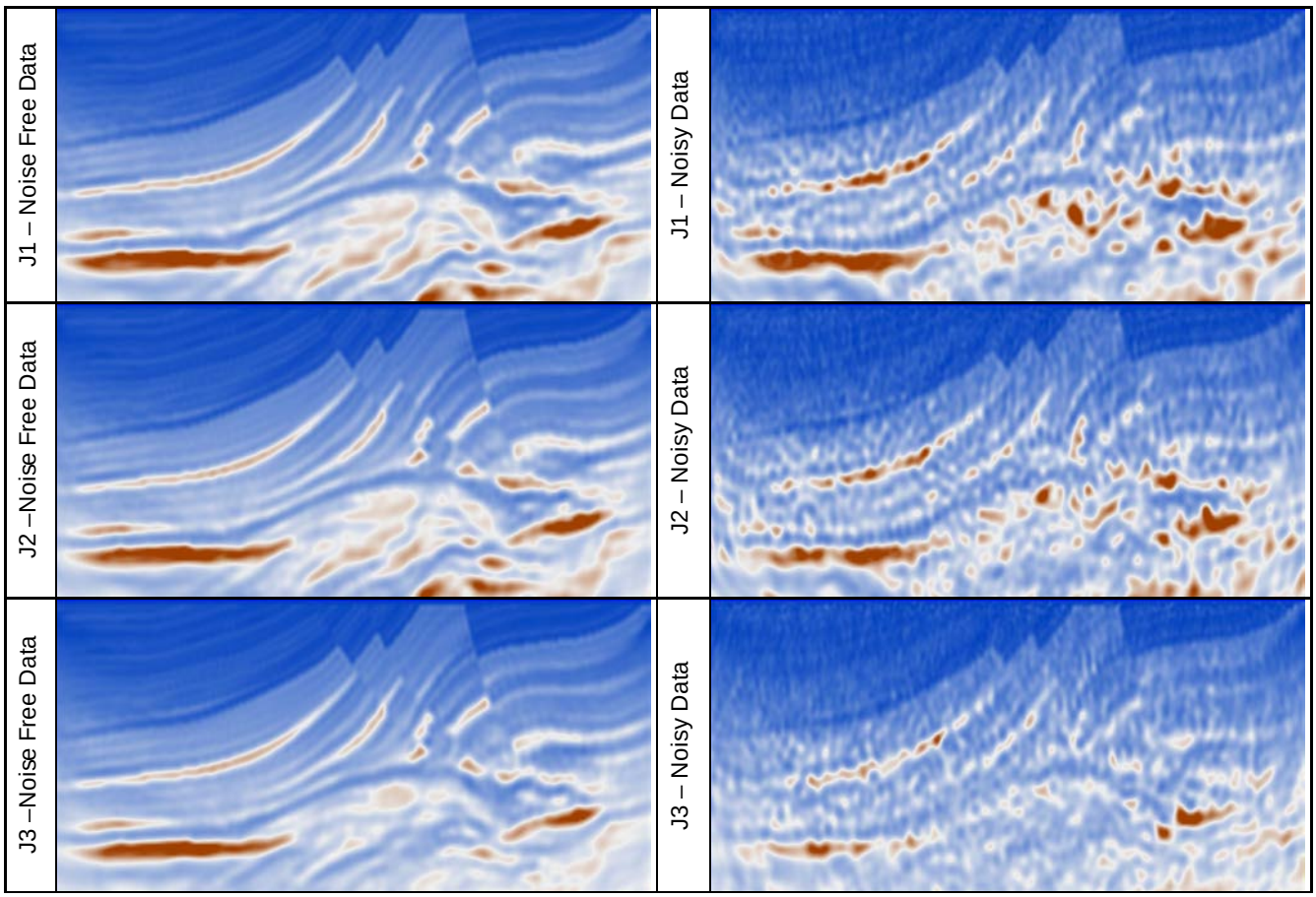

Figure 3 – Final velocity models obtained by the Full Waveform Inversion with different data sets and objective functionals, considering 15 frequencies and 20 iterations per frequency.

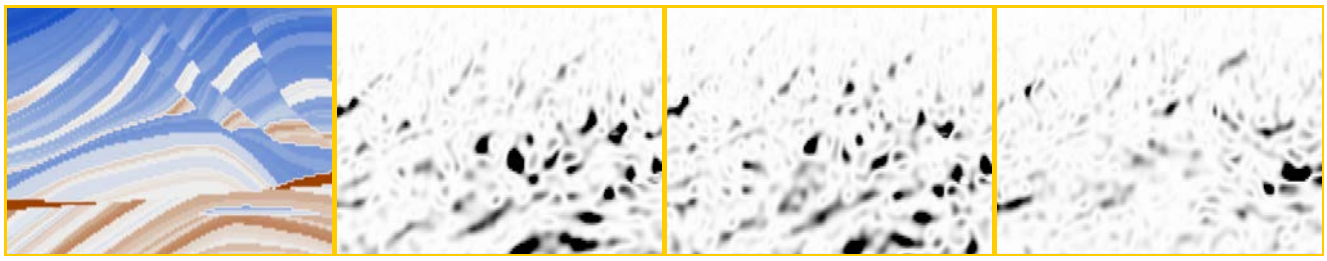

(a) *(b)* *(c)* *(d)*

Figure 4 – Central region for the velocity model (a) and gray scale images of the value of the square difference between results with and without noise for each objective functional, J1 (b), J2 (c) and J3 (d) (darker mean higher differences).